Available online at www.sciencedirect.com
SCIENCE DIRECT
International Journal of Heat and Fluid Flow 26 (2005) 922–930
International Journal of HEAT AND FLUID FLOW
www.elsevier.com/locate/ijhff

Study of periodically excited bubbly jets by PIV and double optical sensors

Rade Milenkovic [a,*], Beat Sigg [b], George Yadigaroglu [b]

[a] Laboratorium für Thermalhydraulics PSI, Paul Scherrer Institut, OVGA 415, CH-5232 Villigen PSI, Switzerland
[b] Laboratorium für Kerntechnik, ETHZ, ETH Zentrum CLT, CH-8092 Zürich, Switzerland

Available online 9 November 2005

Abstract

Interactions between large coherent structures and bubbles in two-phase flow can be systematically observed in a periodically excited bubbly jet. Controlled excitation at fixed frequency causes large eddy structures to develop at regular intervals. Thus, interactions between large vortices and bubbles can be studied with PIV and double optical sensors (DOS) using phase-averaging techniques. A number of results on the time and space dependence of velocities and void fractions are presented revealing physical interactions between the liquid flow field and bubble movement as well as feedbacks from bubble agglomeration on the development of flow structures. A clear indication of bubble trapping inside the vortex ring is the generation of a bubble ring that travels with the same velocity as the vortex ring. The DOS results indicate clustering of the bubbles in coherent vortex structures, with a periodic variation of void fraction during the excitation period.

Keywords: Bubbly jets; Excited jets; Coherent structures; PIV; Optical sensors; Phase averaging

1. Introduction

Dispersed multiphase flows constitute a class of fluid flows of universal importance in process and energy technology as well as in relation with the discharge of waste materials into the environment. Progress has been achieved during recent years in the analysis of two-phase flows mainly because of their increased amenability to numerical simulation, but also due to the availability of more powerful experimental means that enable their detailed study. Because of the limited applicability of direct numerical simulation to technical problems, computational fluid dynamics (CFD) methods, such as the continuous-fluid or point-bubble approach, or more advanced techniques like large eddy simulation (LES) have to be relied upon. These require a great deal of detailed numerical and experimental information for validation (Yadigaroglu and Lakehal, 2003).

To improve physical insight and to support the numerical analyses, a number of basic experiments in bubbly flows have been carried out. In the case of free shear flows, research has been performed on bubbly jets (Iguchi et al., 1995) and plane bubbly mixing layers (Roig et al., 1998). In these tests, the effects of bubble size and concentration on turbulence, velocity and void distributions, shear-layer spreading rates, mixing, characteristic length scales and velocity correlations have been studied. However, these measurements only provide results for statistical properties and the spatial distribution of local stochastic variables and do not deal with spatial coherence and the effects of large structures (vortices), which are very important in shear layers and have been extensively analyzed in single-phase flows (Crow and Champagne, 1970; Ho and Huerre, 1984). In particular, it has been found that phenomena such as the interaction between coherent structures and bubbles, as well as the feedback from bubble agglomeration on the development of these structures, have not been sufficiently explored in experiments whereas many theoretical and numerical analyses exist (Sene, 1994).

* Corresponding author. Tel.: +41 56 310 5147; fax: +41 56 310 4481.
E-mail addresses: rade.milenkovic@psi.ch, rvmil@bluewin.ch (R. Milenkovic).

0142-727X/$ - see front matter © 2005 Elsevier Inc. All rights reserved.
doi:10.1016/j.ijheatfluidflow.2005.10.010

2. Experiment

To contribute to the understanding of the above-mentioned phenomena and to provide experimental information, especially regarding coherent vortex structures, a jet has been periodically triggered to produce coherent structures and to allow phase averaging of the experimental data. Special emphasis had to be attributed to the synchronization of the experimental PIV (particle image velocimetry) measurements, the photographic recordings and the double optical sensor (DOS) measurements with the external triggering of the flow structures. Another unique aspect of the experiment is the use of mono-disperse, controlled-diameter bubbles.

The experiments have been carried out with a vertical water jet containing bubbles of various well-controlled sizes and volume fraction; the jet is injected into a water volume contained in a large Plexiglas tank to minimize wall effects. The gas/liquid injector and a schematic of the experiment (Milenkovic and Fehlmann, 2005; Milenkovic, 2005) are presented in Fig. 1. The injector has been developed after a series of experiments carried out to determine the optimal configuration of tubes and needles for forming bubbles with uniform size in the range between 1 and 6 mm (Milenkovic and Fehlmann, 2005). Bubbles are formed by continuously injecting air (AF) through the needles into the co-currently flowing internal liquid flow—ILF. The jet flow is formed afterwards by adding the second, external liquid flow—ELF.

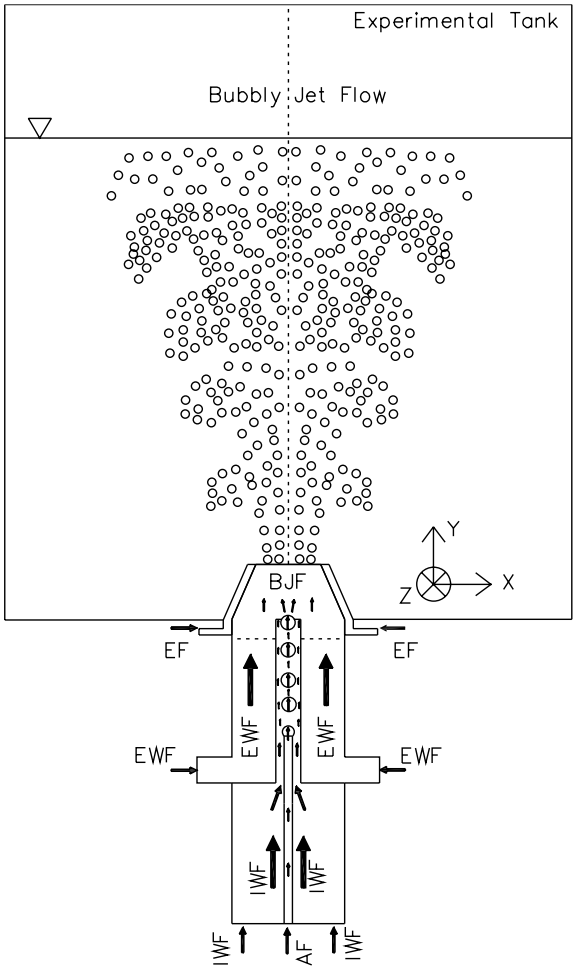

Fig. 1. Schematic of bubbly jet production. The injector shown at the bottom at a much larger scale has 39 injection needles (only one is shown).

As shown in Fig. 1, the injector (Milenkovic and Fehlmann, 2005; Milenkovic, 2005) contains three chambers for, from bottom to top, air injection through the (hypodermic) needles, water injection into the tubes and water injection into the space outside the tubes constrained by a cylindrical shroud called jet nozzle. This nozzle, shown as a conical version, can be exchanged.

An experimental study of the interaction of bubbles with the large-scale structures of the continuous phase of a jet is best accomplished by periodic triggering of the flow with controllable frequency and amplitude. This is achieved by periodically modulating the jet shear layer by means of a coaxial water layer (EF) injected close to the jet exit through a specially designed excitation nozzle, which shrouds the jet nozzle. A fast flow meter is used for measuring the time-dependent flow rate up to frequencies of about 5 Hz. The excitation amplitude can also be adjusted.

The main dimensions and compositions are:

- diameter of the jet: $D = 90$ mm;
- diameter of the tubes: $d_o/d_i = 4.0/3.4$ mm;
- height of the tank: $H = 2240$ mm;
- water level in the tank: $H_L = 1200$ mm;
- width of the tank: $L = 1200$ mm;
- diameter of the excitation nozzle: $D_o/D_i = 98/96$ mm;
- number of tubes and needles: $N = 39$.

Synchronization between PIV, the image acquisition equipment and the triggering device for producing the coherent flow structures was achieved by an encoder mounted on the modulation device. The encoder pulse triggers the PIV system and the DOS high-speed data acquisition.

2.1. Experimental conditions

The results presented here were obtained for a turbulent bubbly jet with mean superficial liquid velocity at the nozzle exit of $V_L = 0.32$ m/s, homogeneous void fraction 3.4% and bubble diameter d of about 2 mm. The triggering frequency f, which corresponds to a jet Strouhal number $St = \frac{D \cdot f}{V_L} = 0.6$, was 2 Hz.

The axial velocity of the EF at the exit of the excitation nozzle for modulated flow rate is shown in Fig. 2. More details about the design of the excitation nozzle can be found in Milenkovic (2005). The experimental techniques are discussed next.

2.2. PIV (particle image velocimetry) and photographic techniques

The standard, commercial PIV system used consists of dual cavity lasers and two CCD cameras that work in a

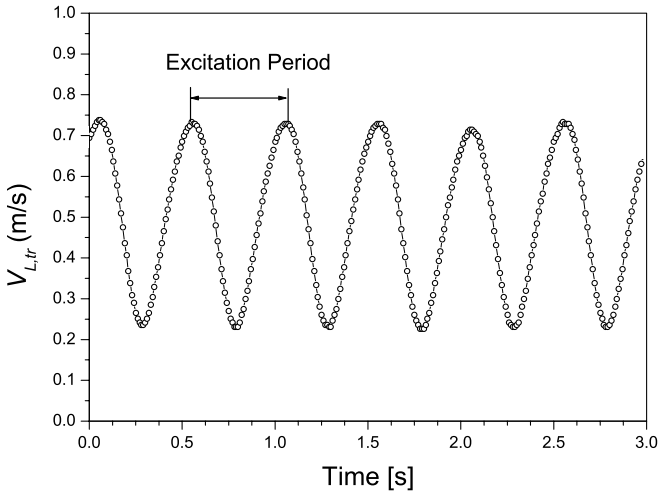

Fig. 2. Modulated triggering velocity.

two-frame double exposure mode. The laser light sheet illuminates a mid-plane of the axisymmetric jet, while the two cameras with the beam splitter are aimed perpendicularly to the laser light sheet. The first camera with a green filter captures reflections from the bubbles, while the second camera with a red filter acquires the images with light emitted from the fluorescent seeding particles used in the experiment. Therefore, the first camera is used for the measurement of bubble velocities, whereas the second one is used for measuring liquid velocities. A special dosing system (barrel, dosing pump and the mixer) is used for feeding the flow with seeding particles. The dimensions of the fields of view used were 138×138 mm and 220×220 mm. For the smaller field of view the optical resolution of 1 pixel corresponded to about 140 μm, and the size of the chosen interrogation area (IA) was 64×64 pixels. This setting was used for obtaining velocity fields of the liquid and of the bubbles. The second field of view was used for estimating the velocity of the vortex and of the bubble ring. Since the good seeding quality was achieved with the dosing system and the time between two laser pulses was adjusted to obtain a maximum particle displacement less than 16 pixels (i.e. 25% of IA), the error of velocity measurements corresponding to a displacement uncertainity of 0.1 pixels is about 1% of the maximum value.

In order to obtain velocity and vorticity fields at various phases within the triggering period, i.e., positions of the vortices in the flow field, a data acquisition scheme has been devised that is synchronized with the excitation (Fig. 3). PIV acquisition is started by the periodic external signal from the encoder (Fig. 3, top), which covers two excitation periods (Fig. 3, middle). The PIV recordings were acquired with higher frequency (in this case 12 Hz). Thus six shots per excitation period are captured, allowing phase-averaging at six different times within the excitation period to be performed (Fig. 3, bottom). The data acquired this way yield information on deformations, size modifications and velocity of the vortex ring. This acquisition method, called here vortex tracking method, is a very useful tool for tracking large vortices in a flow field.

In order to illustrate bubble trapping in shear-layer vortices, the images with bubble reflections (the gas phase) can be phase-averaged and compared with the phase-averaged liquid vorticity field. Since the laser light sheet illuminates 2D intersections of the 3D jet, only bubbles trapped in the shear layer that are illuminated by the laser sheet can be detected.

If one of the two frames captured with the second camera (with the red filter) is illuminated with uniform back-light, the projection of the bubble ring on the image plane can be visualized. In order to simultaneously observe the bubble ring movement and to be able to obtain velocity fields from PIV images, it is preferable to achieve uniform and moderate light intensity of the back-light. Since the intensity of the back-light is negligible with respect to that of the laser, the back-light does not disturb the pictures with reflected laser light from the bubbles obtained with the first camera. On the other side the images from the fluorescent particles should be pre-processed before the PIV analyzing algorithm can be applied as the back-light illumination produced the noise. The histogram plot of light intensity of these images reveals which gray levels belong to the background including bubbles and back-light illumination and which belong to the light emitted by seeding particles. After thresholding, i.e., dividing an image into two pictures (seeding-particle image and a background image), the PIV analysis and cross-correlation algorithm can be applied to obtain the liquid velocity field.

To avoid the risk of adding noise to the PIV pictures and to check both procedures, the experimental acquisition is also performed in two parts: the first half contains standard PIV images and the second one PIV images with back-light illumination. This can be achieved by adding back-light only during the second part of the experiment. Then, the first set of images is used for usual PIV analysis, while the second one is used to observe phase-averaged positions of bubble rings. Since the flow condition was not changed and image acquisition was not stopped, the data obtained in this way could be compared.

If the flow field is illuminated additionally by the back-light and if the acquisition scheme presented is applied, it is possible to observe the movement of the bubble ring and to estimate its velocity. Therefore it is possible to compare vertical velocity of the vortex ring and of the bubble ring.

2.3. Double optical sensor (DOS)

A standard instrument often used in bubbly flows is the double optical sensor. Void fraction (ε), number of bubbles (N), bubble chord length distribution, as well as vertical bubble velocity (V_B) can be measured by DOS.

In general, the DOS-measured bubble velocities depend on many factors such as sensor response, sensor geometry, bubble shape and bubble velocity fluctuations. The double optical sensor used for void fraction and bubble velocity

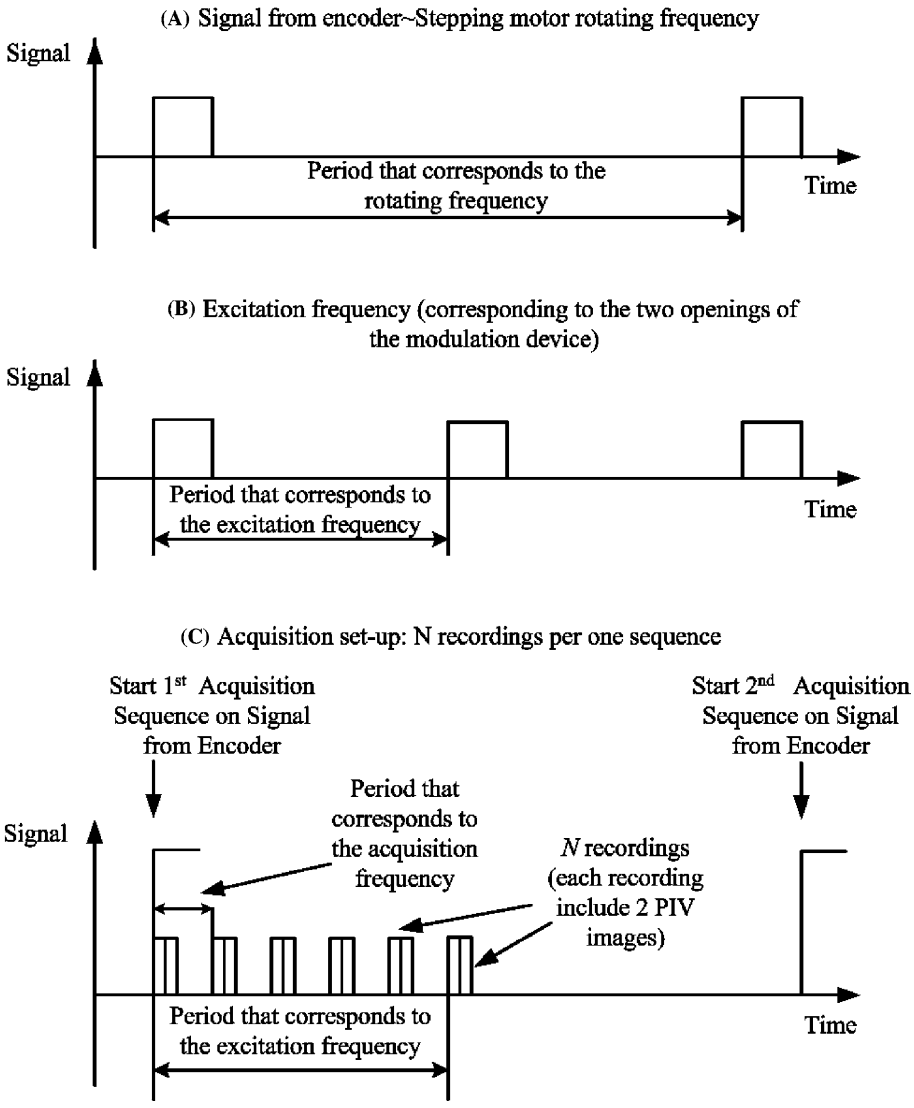

Fig. 3. PIV triggering acquisition scheme.

measurements was horizontally oriented and had a vertical distance between tips of $\Delta y_{\text{tips}} = 0.75$ mm but no horizontal displacement Δx_{tips} (Kubasch, 2001).

During this study it was found that bubble velocity results obtained by DOS always over-estimate PIV data. The basic principles and differences of both techniques, accompanied with a comparison of results for typical turbulent flow conditions with high bubble concentration, are pointed out in more detail in Milenkovic (2005). The main reason for overpredicting the velocity is that bubbles with a relatively large horizontal velocity component lead to a short time delay, which is erroneously interpreted as a high axial velocity. Furthermore, for small ratio $\Delta y_{\text{tips}}/d$, the probability of hitting both tips with the front surface of the bubble within a short time interval can be relatively high, which leads to overprediction of the velocity, contrary to the case $\Delta y_{\text{tips}}/d > 1$. Obviously, the described phenomenon depends on the flow conditions. The resulting biassing effect on the velocity measurements can be minimized by an optimum choice of the DOS geometry, but it cannot be eliminated. A statistical analysis shows that the bubble velocity fluctuations cannot be neglected, and therefore an over-estimation of the bubble velocity of up to 30%, as reported in Le Corre and Ishii (2002), can result.

In order to enable phase averaging of the DOS data, the acquisition was started by the external encoder signal and was stopped after 6000 periods containing data. Each period was divided into 25 intervals of 0.02 s for an excitation period of 0.5 s. The bubble number, void fraction and vertical bubble velocity data were phase-averaged for each of the intervals. The average number of bubbles counted per interval was about 100. The statistical error for the calculated phase-averaged void fractions therefore is about 10%. Measurements were performed at $y = 50$, 100 and 200 mm downstream of the jet exit at radial positions $x = 48$, 50 and 52 mm in the shear layer.

3. Results and discussion

The experimental techniques described above were used to study the entrapping of bubbles in the vortices created in externally and periodically jets.

In order to study interactions between bubbles and large eddies formed in the shear layer and especially bubble trapping phenomena, it was necessary to formulate a simplified condition that should be fulfilled for bubble trapping and to predict the corresponding flow parameters. Obviously, despite the fact that flow conditions for bubble trapping vary in the flow field, the simplified approach, which is presented in more detail in Milenkovic (2005), can be used to check if the conditions for bubbles reaching an equilibrium position in large vortices are fulfilled.

A simplified straight vortex with axis normal to the buoyancy direction and the laser light sheet is considered and the forces acting on a single bubble are formulated. Trapping of the bubble is then defined as the existence of an equilibrium position of the bubble inside the vortex. A more general form of trapping is that of a bubble moving inside a vortex (Sene, 1994; Eames and Magnaudet, 2000).

The vorticity ω_z, which has approximately Gaussian shape, is defined as $\omega_z = \omega_o \cdot e^{\frac{-r^2}{R_v^2}}$, where R_v is the vortex radius and ω_o is the vorticity in the vortex center. The four forces buoyancy (**B**), drag (**D**), inertia (**I**), and lift (**L**), determine bubble movement in the flow field (Fig. 4). U_φ is the circumferential velocity of the liquid relative to the vortex center.

At an equilibrium position of the bubble inside the vortex, the sum of radial as well as azimuthal components must be zero. For such a position two quantities have been deduced from the balance of forces acting on bubbles: the vortex trapping parameter, defined as $\Gamma_\omega = \frac{\omega_o \cdot R_v}{V_T}$, and the vortex Froude number $Fr_\omega = \frac{\omega_o^2 \cdot R_v}{4 \cdot g}$, where V_T is the terminal bubble rise velocity. These parameters indicate whether, for a chosen flow situation, the condition for bubble trapping is approximately fulfilled or not. This trapping condition requires certain values that depend on terminal bubble rise velocity (V_T) and vortex size (R_v). The minimum values for Γ_ω and Fr_ω that must be exceeded for trapping to occur are plotted in Fig. 5 as functions of $Fr_b \cdot \beta$, where $Fr_b = \frac{V_T^2}{2 \cdot g \cdot d}$ is the bubble Froude number, $\beta = \frac{d}{2 \cdot R_v}$ the length scale ratio and d is the bubble diameter.

In order to estimate these quantities, it is necessary to measure liquid velocities at the mid-plane of a vortex ring and to calculate the resulting vorticity (ω_z) and vortex radius (R_v).

The phase-averaged profiles of the vorticity (ω_z) presented in Fig. 6 show the existence of large elliptical Gaussian vortex structures in the shear layer. The peak vorticity at the vortex center is about 60 s^{-1}.

The vortex radius R_v estimated from the phase-averaged azimuthal vorticity field at $y = 50$ mm is about 13 mm (parameter a presented in Fig. 6). The terminal bubble rise velocity V_T for 2 mm bubbles is 0.26 m/s. Based on these values the vortex trapping parameter is $\Gamma_\omega = 3$, while the vortex Froude number is $Fr_\omega = 1.2$. Since the minimum values of these parameters for bubble trapping are reached ($\Gamma_\omega = 2.7$ and $Fr_\omega = 1.2$ for $Fr_b \cdot \beta = 0.13$), the trapping conditions are fulfilled. Furthermore, with the vertical vortex "radius" ($b = 16.5$ mm) one obtains the vortex trapping parameter $\Gamma_\omega = 3.81$ and the vortex Froude number $Fr_\omega = 1.5$ which are larger.

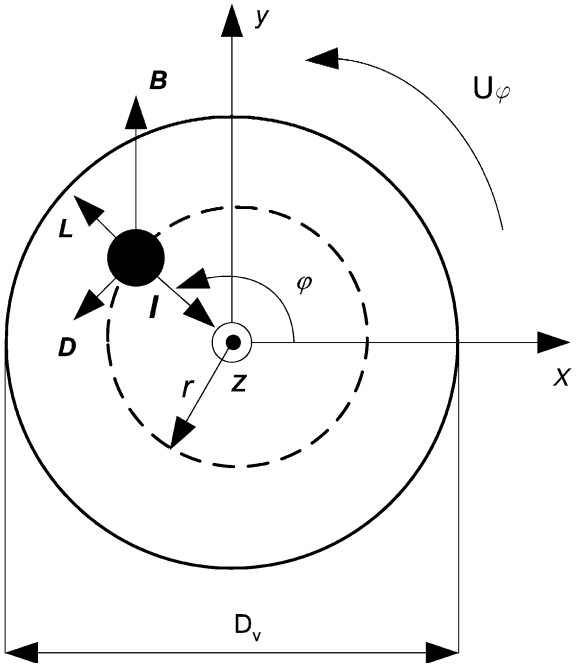

Fig. 4. Forces acting on a single bubble in a vortex.

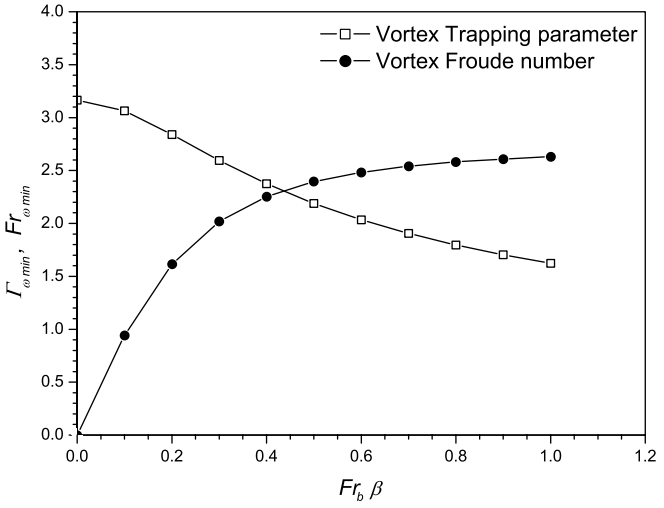

Fig. 5. Minimum values of the vortex trapping parameter and of the vortex Froude number required for trapping bubbles in axisymmetric Gaussian vortex.

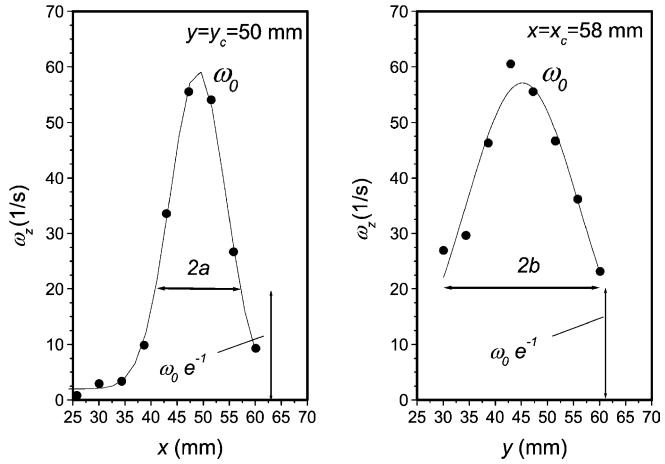

Fig. 6. Horizontal and vertical profiles of the vertical phase-averaged azimuthal vorticity through the center of the vortex in the shear layer.

3.1. Phase-averaged velocity fields obtained by PIV

Fig. 7a and b shows results, such as phase-averaged vertical liquid (V_L) and bubble velocity (V_B), standard deviation of vertical liquid velocity ($StdevV_L$) and azimuthal vorticity of the liquid (ω_z) obtained by PIV at $y = 50$ mm and 100 mm downstream of the jet exit, respectively. The first selected level corresponds to the mid-plane of a vortex ring (Fig. 9a) formed in the shear layer around the jet, while the second lies in the middle between the vortices in the shear layer.

Equality of vertical liquid velocity V_L at the vortex center with bubble velocity V_B close to this center indicates trapping (Fig. 7a, top).

The phase-averaged value of the standard deviation of the vertical liquid velocity $StdevV_L$ (Fig. 7a and b, bottom) corresponds to the incoherent part of vertical velocity fluctuations.

In between the vortices, the shear layer is much broader and vorticity is produced by the mean shear (as shown in Fig. 7a and b, middle).

The PIV phase-averaged image of bubble reflections (obtained by superimposing several shots synchronized with vortex triggering and filtered with the Max Pixel Operator technique (Milenkovic, 2005)) presented in Fig. 8 illustrates bubble clustering inside the large vortices. Bubbles that are illuminated by the laser sheet reflect light. The increased bubble concentration (Fig. 8) inside the large vortices may indicate bubble trapping.

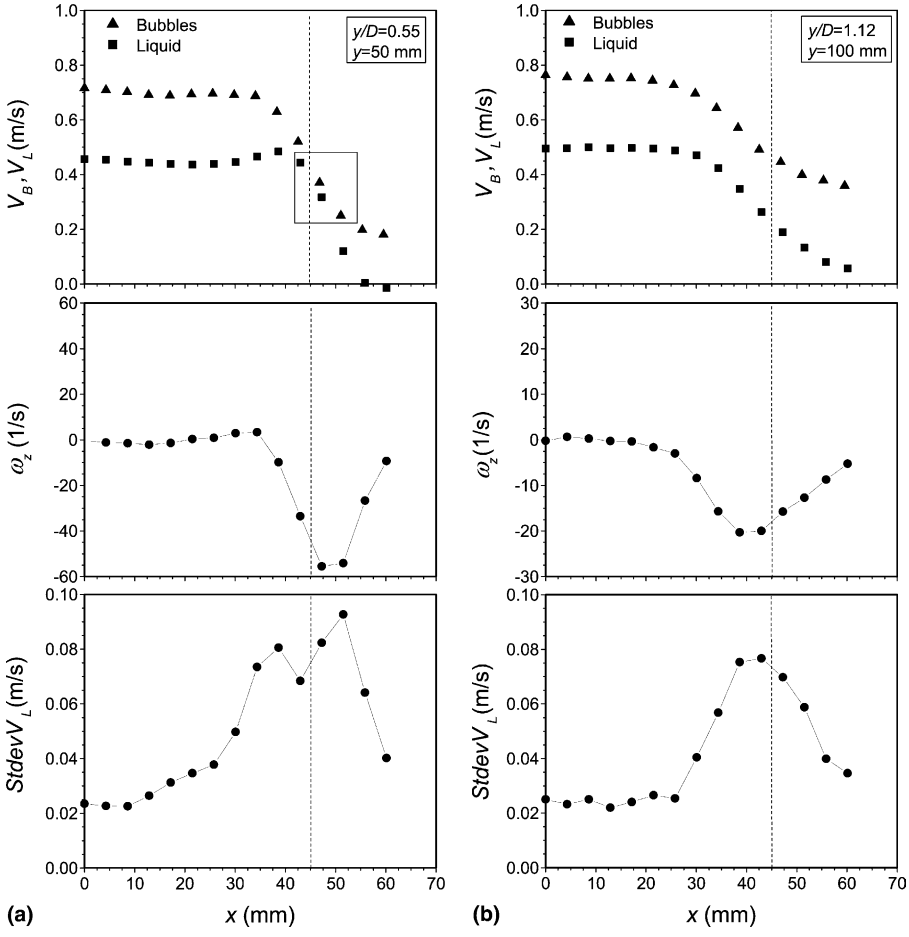

Fig. 7. Horizontal profiles of phase-averaged vertical velocity (top), standard deviation of vertical velocity (bottom) and azimuthal vorticity (center) of the liquid through the center of the vortex in the shear layer (a) and between the vortices in the shear layer (b).

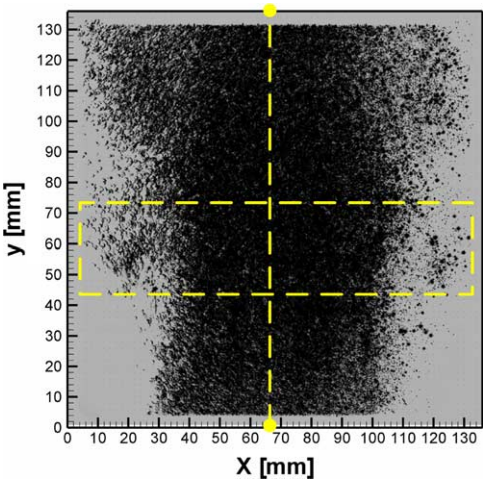

Fig. 8. Phase-averaged image of bubble reflections in the observation window.

A clear indication of bubble trapping inside the vortex ring is the generation of a bubble ring (Fig. 10) that travels with the same velocity as the vortex ring. The velocities of both vortex and bubble ring can be estimated from the data acquired by the PIV vortex tracking method with or/and without illumination of the flow field with back-light. Furthermore, visualization tests show strong deformations of the bubble ring due to instabilities in the shear layer (Fig. 10).

An example of results obtained by vortex tracking acquisition is presented in Fig. 9. The contour map of the phase-averaged azimuthal vorticity of the liquid obtained by PIV measurement, presented in Fig. 9a, shows the position of the same vortex ring as in Fig. 9b but shifted downstream by about 68 mm for a phase shift is 250 ms. The resulting vortex velocity of about 0.27 m/s agrees with the estimated bubbly ring velocity.

In general, the appearance of bubble rings reveals that bubbles are trapped in the vortex rings, since both have about the same velocity. The presented PIV technique is found to be a powerful tool for observing bubble trapping inside large vortices.

3.2. Phase-averaged void fraction and vertical bubble velocity measured by DOS

The DOS point measurements have been conducted at different positions in the shear layer with excitation. Phase-averaged results of DOS measurements in the shear

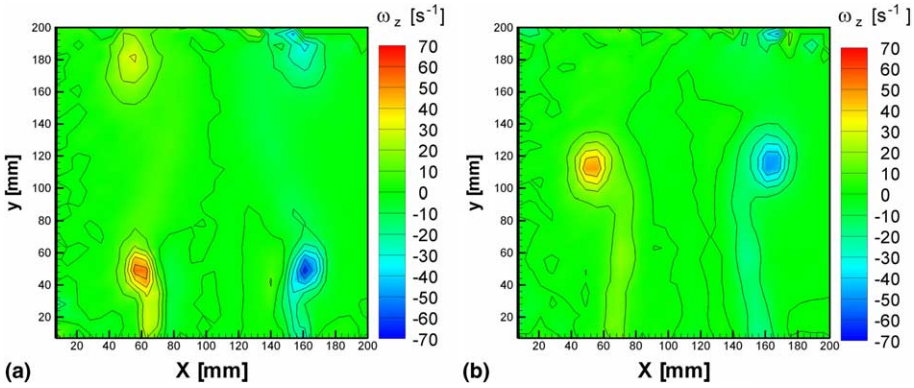

Fig. 9. Phase-averaged azimuthal vorticity field of the liquid. Vortex ring is located close to the jet exit (a), whereas downstream position of the same vortex ring after a phase shift of 250 ms is shown in scalar map (b). The jet centerline is at $X = 108$ mm.

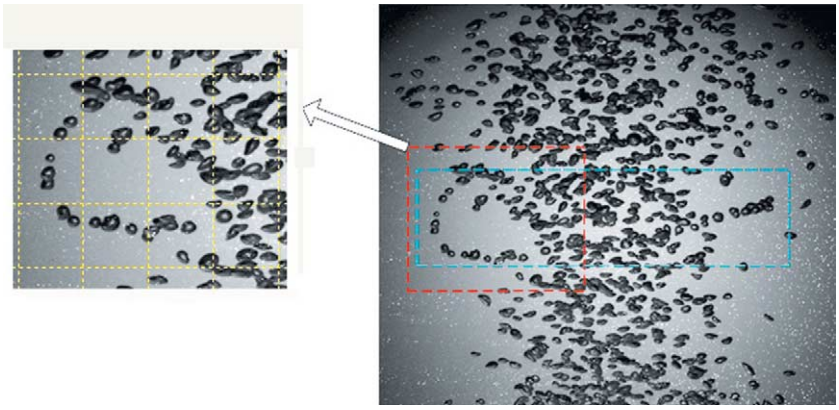

Fig. 10. Photograph of the bubbles trapped in a vortex ring.

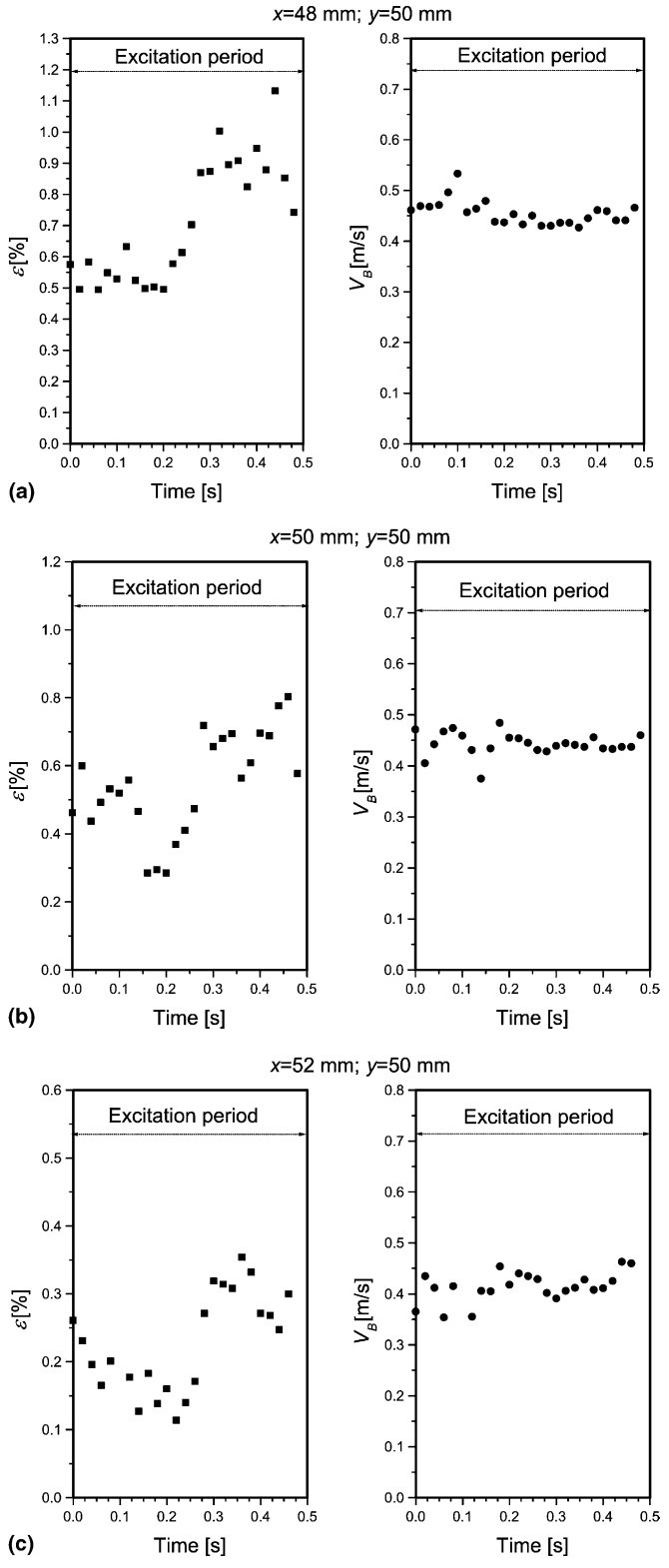

Fig. 11. Phase-averaged void fraction and vertical bubble velocity measured with DOS during an excitation period at $y = 50$ mm and $x = 48$ mm (a), $x = 50$ mm (b) and $x = 52$ mm (c).

layer extending over the full excitation period of 0.5 s are presented in this section. Since the velocity of the vortex ring obtained by the PIV vortex tracking method is about 0.27 m/s, the time interval chosen for data analysis of 0.02 s corresponds to a vertical distance of about 5.5 mm. The void fraction generated by trapped bubbles would then be averaged over $\Delta y = 5.5$ mm, which is comparable to the bubble size. Therefore, this resolution should be adequate for distinguishing trapped from non-trapped bubbles in ensemble-averaged void fraction and bubble velocity distributions. The vortex ring shown in Fig. 9a is formed at about 30 mm from the nozzle exit, which means that a bubble ring exists at the DOS tips at $y = 50$ mm.

Fig. 11 shows phase-averaged results of DOS measurements for points in the shear layer ($x = 48$, 50 and 52 mm) at $y = 50$ mm downstream of the jet exit. The results indicate clustering of the bubbles in coherent vortex structures, since the void fraction strongly varies during the excitation period. Results also show the time-dependence of the bubble velocity during an excitation period.

Fig. 12 shows the void fraction and vertical bubble velocity for the same horizontal location in the mixing layer but at different vertical elevations, illustrating the phase shift between the different positions. The existing phase shift between these points corresponds to the downstream vertical velocity of the vortex ring. The time delay between the void fraction maxima (ε_A and ε_B) presented in Fig. 12, respectively is about 0.37 s. The vertical distance between the two locations is 100 mm. Thus, the estimated downstream traveling velocity of the bubble structures is about 0.27 m/s, which is in agreement with the value obtained by PIV for the vertical vortex ring velocity.

In some cases it may be possible to identify the bubble ring by means of the DOS technique, because the lower peak in Fig. 12 (left) could be caused by a small cluster of bubbles, also shown in Fig. 8. Furthermore, it must be emphasized that the bubble ring position fluctuates and the bubble concentration is averaged over a vertical interval of about 5–10 mm. The bubble rings do not lead to high mean bubble concentration, but they can give rise to a detectible bubble cluster within the period of excitation. Nevertheless, the DOS technique alone cannot be used to detect bubble trapping. It can only be shown that the measurements are consistent with PIV and shadowgraphy results if bubble trapping occurs.

4. Conclusions

Controlled excitation at fixed frequency and with defined amplitude, achieved by producing small flow surges around the jet nozzle, causes large eddy structures to develop at regular intervals. The production of externally triggered coherent structures as well as synchronization with data acquisition, is found to be a useful tool for the observation of bubble movement that cannot be achieved in naturally developing jet flows. Furthermore, the systematic control of inlet conditions makes this experiment a state-of-the-art platform for exploring complex phenomena occurring in bubbly flows.

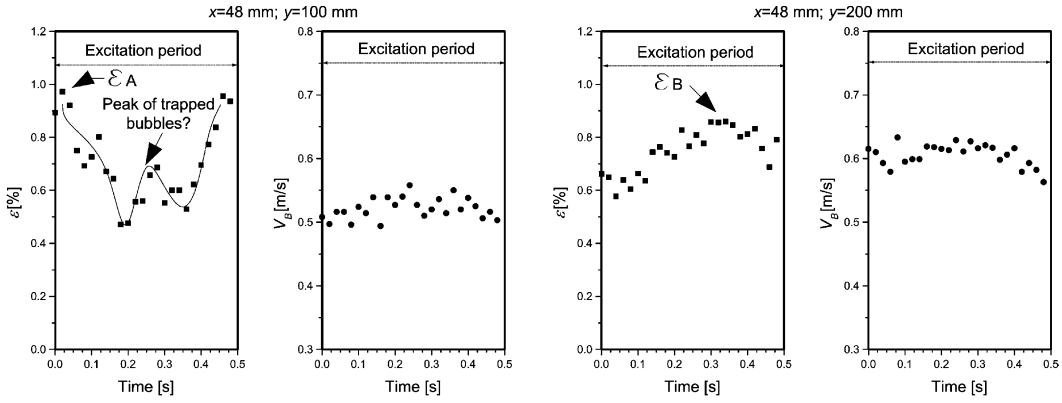

Fig. 12. Variation of the phase-averaged void fraction and of the vertical bubble velocity measured with DOS during the excitation period at $y = 100$ mm (left) and 200 mm (right) and at $x = 48$ mm.

The experiment shows how PIV and DOS techniques can be applied in a triggered two-phase flow experiment. The generation of a bubble ring that travels with the same velocity as the vortex ring is a clear indication of bubble trapping inside the vortex ring.

Acknowledgments

The authors gratefully acknowledge the support of the project by the Swiss National Science Foundation under Contract No. 200020-103630 and wish to thank Max Fehlmann for his helpful assistance and technical contributions to the design and erection of the experimental installation.

References

Crow, S.C., Champagne, F.H., 1970. Orderly structure in jet turbulence. J. Fluid Mech. 48 (3), 547–591.

Eames, I., Magnaudet, J., 2000. The motion of high-Reynolds-number bubbles in inhomogeneous flows. Ann. Rev. Fluid Mech. 32, 659.

Ho, C.M., Huerre, P., 1984. Perturbed free shear layers. Ann. Rev. Fluid Mech. 16, 365–424.

Iguchi, M., Ueda, H., Uemura, T., 1995. Bubble and liquid flow characteristics in a vertical bubbling jet. Int. J. Multiphase Flow 21, 861–873.

Kubasch, J., 2001. Bubble Hydrodynamics in Large Pools. Doctoral thesis no. 14398, ETH Zürich, Switzerland.

Le Corre, J.M., Ishii, M., 2002. Numerical evaluation and correction method for multi-sensor probe measurement techniques in two-phase bubbly flow. Nucl. Eng. Des. 216, 221–238.

Milenkovic, R., 2005. Experimental Investigation of Bubbly Jets. Doctoral thesis no. 16206, ETH Zürich, Switzerland.

Milenkovic, R., Fehlmann, M., 2005. Gas/liquid injector (mass and/or heat transfer apparatus and method for mass and/or heat transfer enhancement), pending European Patent (PSI and ETHZ patent application no. 2003P19217EP (F-5125)).

Roig, V., Susanne, C., Masbernat, L., 1998. Experimental investigation of a turbulent bubbly mixing layer. Int. J. Multiphase Flow 24, 35–54.

Sene, K.J. et al., 1994. The role of coherent structures in bubble transport by turbulent shear flows. J. Fluid Mech. 259, 219–240.

Yadigaroglu, G., Lakehal, D., 2003. New challenges in computational thermal hydraulics, invited plenary lecture. In: The 10th International Topical Meeting on Nuclear Reactor Thermal Hydraulics (NURETH-10), Seoul, Korea, October 5–9.